ELSEVIER

Dynamics of Atmospheres and Oceans
31 (2000) 1–21

dynamics of atmospheres and oceans

www.elsevier.com/locate/dynatmoce

Circulation and boundary layers in differentially heated rotating stratified fluid

J.A. Whitehead *, J. Pedlosky

Department of Physical Oceanography, Woods Hole Oceanographic Institution, MS #21, 360 Woods Hole Road, Falmouth, MA 02543-1541, USA

Received 28 August 1998; received in revised form 5 January 1999; accepted 12 April 1999

Abstract

Recent laboratory experiments with rotating stratified water in a cylinder have revealed many of the predictions of linearized, analytic theory. Earlier measurements of the velocity field generated in a cylinder by top heating compared well with theory. Large stratification clearly suppressed Ekman pumping so that the interior velocity field (primarily azimuthal) responded by satisfying no-slip top and bottom boundary conditions without the need for Ekman layers. This interior flow also occupied a boundary layer of greater thickness than the Ekman layer under some conditions. Theory and experiments have now been conducted for sidewall heating. As before, experiment and theory agree well over some parameter ranges. But for some parameters, the flow is unstable. The exact nature of the instability remains poorly understood. The size of one combination of both vertical and horizontal boundary layers is governed by the Rossby radius of deformation multiplied by the square root of the Prandtl number. Sidewall boundary layers and their scales will be reviewed with the present results in mind.

Keywords: Circulation; Boundary layer; Stratified fluid

1. Introduction

There are many ocean and marginal sea basins with lateral size less than 1000 km, but which are large enough to be effected by the Earth rotation. In many of these, the small widths compared to Earth's radius may negate the well-developed theories of the wind-driven thermocline or the theory of large-scale abyssal circulation. To a first

* Corresponding author. E-mail: jwhitehead@whoi.edu

0377-0265/00/$ - see front matter
PII: S0377-0265(99)00026-3

approximation, one might assume that the flows are influenced both by Earth rotation and stratification of the water. These can be set to constant values for simplicity.

Many dynamical studies attack one or two isolated aspects of circulation in a mesoscale stratified basin. One set, as an example was motivated by observations that surface circulation in numerous lakes and inland seas is frequently cyclonic. A number of mechanisms involving wind and thermal effects were hypothesized to produce this sense of circulation (Emery and Csanady, 1973; Wunsch, 1973; Bennett, 1975; Csanady, 1976, 1977). Another mechanism for generating cyclonic circulation arises from freshwater currents from rivers which deflect to the right in the Northern Hemisphere to form buoyant outflows so that the freshwater density current leans against the right hand wall and propagates in a cyclonic direction (Takano, 1955) with respect to the interior. This has been studied experimentally (Whitehead and Miller, 1979; Stern et al., 1982; Griffiths and Hopfinger, 1983; Griffiths, 1986; Whitehead and Chapman, 1986) and theoretically (Garvine, 1974, 1987, 1996; Stern, 1980; Chao and Boicourt, 1986; Wang, 1987; Chao, 1988; O'Donnell, 1990; Masse and Murthy, 1992; Munchow and Garvine, 1993; Chapman and Lentz, 1996; Kourafalou et al., 1996; Yankovsky and Chapman, 1997, among others). These mimic the surface adjustment problem studied theoretically by Gill (1976). Circulation at mid and bottom depths are partially influenced by stream tubes (Smith, 1975; Price et al., 1993; Chapman and Lentz, 1994; Johnson et al., 1994a,b; Jungclaus and Backhaus, 1994; Spall and Price, 1998) which are discussed mostly in the context of the large oceanic outflows (Whitehead, 1989) but which, in a modified (and perhaps very weak) form, are found in a number of mesoscale basins such as the Black Sea (Latif et al., 1991), Caribbean seas (Stalcup et al., 1975; Sturges, 1975; Fratantoni, private communication, text in preparation) and Arctic Ocean (Aagard, 1981; Krysell and Wallace, 1988).

To give some examples, the deep circulation of the Black Sea is poorly understood compared to the understanding of the surface flows. A first approximation of the deep flow in the form of sidewall-driven buoyancy-driven flow has been advanced by Bulgakov (1987) and Bulgakov and Korotaev (1987). It was developed further by Bulgakov et al. (1996a) and observed in laboratory studies (Bulgakov et al., 1996b; Whitehead et al., 1998). The circulation of the Arctic basin is well-known to be anti-cyclonic in the upper few hundred meters and deeper flow is reported to be cyclonic (Aagard, 1981). But current meter or drifter data that illustrate the actual pattern of deep circulation in the Arctic ocean are absent. Detailed circulation patterns of the deep waters in other marginal seas such as the Caribbean, Indonesian basins, and Mediterranean basins are also only slightly documented at present. Circulation in the deepest and remotest small basins — deep ocean trenches — is virtually unknown, although there is some recent evidence of cyclonic recirculation over and within the trench (Johnson, 1998).

One appropriate starting dynamical balance for the flow arises from the analytical study by Barcilon and Pedlosky (1967a; b; c) (also given in Pedlosky, 1979, Chap. 8.3), where the role of assorted boundary layers and their contribution to circulation was studied in a rotating cylinder of linearly stratified fluid. The flows thereby include some effects of temperature advection, but since they obey linearized equations, they can be analytically studied in some detail.

A recent comparison between laboratory measurements and calculations (Pedlosky et al., 1997) resulted in a good view of circulation driven by a radially heated lid which, for all practical purposes, was insulated along the sidewall. The dependence of the flow structure and magnitude upon three dimensionless numbers gives some quantitative guidance about the internal structure of the flow field. There is decent quantitative agreement between experiment and theory in the range for which the theory is expected to be valid. Prominent among the results is that for large stratification, a boundary layer at the top boundary has a thickness such that the Rossby radius of deformation defined by this thickness times the square root of the Prandtl number is roughly equal to tank radius. The layer has been observed in some detail. Another feature of this layer is that for large stratification, velocity in this layer approaches a small value at the edge of the top Ekman layer, largely expunging the role of the Ekman layers.

The experiment (Fig. 1) consisted of heating a rotating, stably stratified cylinder of fluid from above with a radially varying surface temperature distribution. The fluid was

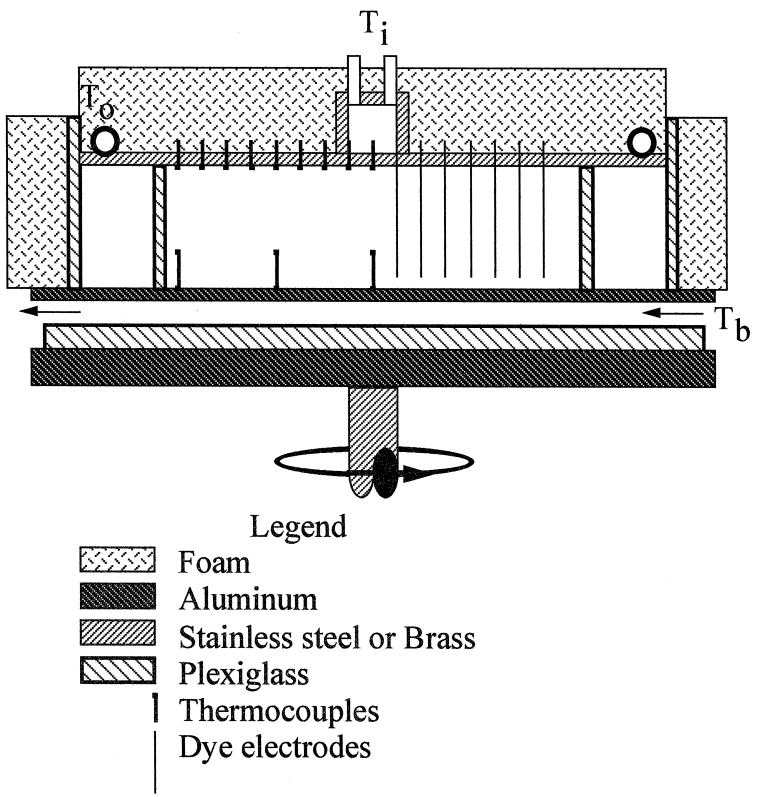

Fig. 1. Sketch of the apparatus used by Pedlosky et al. (1997) to investigate circulation in rotating stratified water with a radial temperature distribution on the top lid. Three baths, denoted by subscripts i, o, and b, provided fixed temperatures at the top center, top outer radius and all along the bottom, respectively. The dye electrodes produced vertical columns of dye that were distorted by azimuthal flow so velocity profiles could be obtained.

also given a colder constant temperature along its bottom boundary. The desired temperature distribution was created with three baths. The bath feeding the metal covered chamber along the bottom was set to a steady cold temperature T_b. A second bath was set at a much higher temperature and fed water into the center of a top lid at temperature $T_i = T_b + \Delta T_v$. A third bath fed water into the outer rim of the lid at a slightly different warm temperature $T_0 = T_b + \Delta T_v + \Delta T_h$. ΔT_h produced a lateral temperature distribution along the top of the test fluid that, with thermal wind, created a vertical shear in the test fluid immediately under the lid. That shear then drove flows which were measured for comparison with calculations. Theory and experiments agreed qualitatively well over a large parameter range. Quantitative comparison was also very good.

Scaling considerations show that a wide range of parameters which are useful for atmospheric and ocean dynamics can be attained in the laboratory with such experiments. The independent variables are acceleration due to gravity g, coefficient of thermal expansion α, vertical temperature difference ΔT_v, lateral temperature difference ΔT_h, radius R, depth L, Coriolis parameter f, viscosity μ, density ρ and thermal diffusivity κ; these produce four dynamically important dimensionless numbers. We select the first one to be $S = g\alpha\Delta T_v/f^2L(= N^2/f^2)$, the square of the ratio of Rossby radius of deformation to radius of the tank. Using values of $g = 1000$ cm^2 s^{-1}, $\alpha = 2\times10^{-4}$°C^{-1}, L ranging from 5 to 50 cm, ΔT_v from 2 to 40°C, f from 10^{-4} to 3 s^{-1}, S varies from 0.001 to 10^8. In the ocean, typical values of N/f are from about 1 to 100; thus, S would range from about 1 to 10,000 so there is considerable overlap between ocean and laboratory values. Ekman number $2\mu/\rho fL^2$ is the second parameter. It can range from about 10^{-3} to greater than 1 in the laboratory and from 4×10^{-6}, up to 0.01 in the ocean (using a ''turbulent'' value for the diffusion of momentum). The third dimensionless number is Prandtl number $\sigma = \mu/\rho\kappa$ which is order one in the laboratory and probably so in the ocean, too. Based upon these three dimensionless numbers, there is hope that these results will bear upon the actual circulation in small deep basins. The fourth number expresses the strength of the flow, a Rossby number $Ro = U/fR$ can express this. In the laboratory, using a typical velocity of 0.07 cm s^{-1} (this speed can be found in Section 3) and a 7-cm radius, Ro is from 0.003 to about 100 using the range of f given above. In the ocean, using a typical velocity of 0.1 m s^{-1}, basin radius R varies from 10 to 1000 km, so Rossby number ranges from 0.001 to 0.1, and there is overlap over at least one decade. This can is also be expressed as the thermal Rossby number $R_T = g\alpha\Delta T_h L/f^2R^2$ which takes the values 0.01 to 100.

Barcilon and Pedlosky find a number of interesting boundary layers and explore their dynamical effects which such experiments can seek to demonstrate. Some of them are similar to boundary layers developed by Veronis (1967), who emphasized analogies between rotating and stratified fluids subjected to thermal and stress forcing. But others involve the combined effects of rotation and stratification, and are thereby not included in the analogy. The predicted existence of a ''rotating stratified'' boundary layer and its role in determining the structure of the flow for strongly stratified flow was confirmed in the experiment. For top lid thermal driving, flow is structured as follows: For $\sigma S \ll 2E^{1/2}$, stratification is small compared to rotation. Interior flow consists of vertical flow w produced by Ekman layer pumping in the top and bottom boundary layers. The

vertically constant w acting with the zeroth order stratification generates interior temperature that produces interior azimuthal flow v through thermal wind. In contrast, if stratification is large ($\sigma S \gg 2E^{1/2}$), w is hindered by stratification and becomes confined to a boundary layer. The boundary layer's depth δ is such that $\sqrt{\sigma} N\delta/f = R$. Although the boundary layer possesses both viscous and thermal driving, its size is only weakly determined by dissipative mechanisms since only the square root of the Prandtl number (which we expect to be about 1) determines its depth. Over a wide range of parameters, the magnitudes of velocity maxima in the theory agreed with experimental measurement.

Sidewall boundary layers played no role in the above investigation as they are not important when temperature is imposed along the top or bottom surfaces in conjunction with zero heat flux sidewall boundary conditions. If temperature is imposed along the sidewalls, a new set of boundary layers become important. They have not been investigated in detail in the past. It is these boundary layers and the role they play in establishing interior flows which we investigate here.

2. Theory

We are interested in developing a model for the circulation of a stratified fluid in a small ocean basin when the fluid is driven by a concentrated buoyancy source on the outer rim of the cylinder. We represent the source as an axially symmetric heating concentrated at a particular elevation on the outer cylinder rim. The principal difference between this model and the one studied earlier by Pedlosky et al. (1997) is that the interior motion in the sidewall boundary layer is now vital to the dynamics of the fluid, in contrast to the case studied before when the fluid was heated from above. The heating at the sidewall forces a vertical mass flux in the sidewall boundary layer. The divergence of this mass flux sucks fluid from the interior into the boundary layer and the radial motion thus produced in the interior will drive the azimuthal interior velocity which is the largest velocity of the motion field (and the principal signal observed in the experiments described in Section 3).

The motion in response to the heating is assumed to be axially symmetric and the governing equations, as in Pedlosky et al., are taken as linearized about a constant background temperature gradient which provides a spatially constant static stability. In non-dimensional units, the equations of motion are:

$$-v = -p_r + \frac{E}{2}\left[\nabla^2 u - \frac{u}{r^2}\right], \tag{2.1a}$$

$$u = \frac{E}{2}\left[\nabla^2 v - \frac{v}{r^2}\right], \tag{2.1b}$$

$$O = -p_z + T + \frac{E}{2}\nabla^2 w, \tag{2.1c}$$

$$O = \frac{1}{r}(ru)_r + w_z, \tag{2.1d}$$

$$Sw = \frac{E}{2\sigma}\nabla^2 T. \tag{2.1e}$$

The parameters were defined in Section 1 as $S = g\alpha\Delta T_v/f^2 L$ where L is the depth of the fluid in the cylinder, the Ekman number, $[E = 2\mu/\rho f L^2]$ which is presumed small, and $\sigma = \mu/\rho\kappa$ the Prandtl number. The temperature is scaled in terms of the rate of heat addition provided by the concentrated source at the outer boundary at radius r_0. If this source is Q_j in magnitude, the temperature anomaly, i.e., the departure from the background stratification is scaled by:

$$\Delta T_h = \frac{Q_j}{2\pi r_0 k}. \tag{2.2}$$

Here, k is the thermal conductivity. The velocity is scaled according to the thermal wind relation so that the scale for the velocity is $U = (g\alpha\Delta T_h/f)$. Lengths are scaled with the cylinder depth L.

It is useful to divide the fluid domain into an interior and a region in which boundary layer dynamics apply. Along the horizontal boundaries of the cylinder, Ekman layers will exist for all $\sigma SE \ll 1$. On the side wall of the cylinder, for $\sigma S \gg E^{1/2}$, there is a boundary layer of non-dimensional thickness $\delta_b = E^{1/2}/(\sigma S)^{1/4}$. This is the buoyancy layer described in Barcilon and Pedlosky (1967a). In the region outside these boundary layers, it is easy to show that the azimuthal velocity is in geostrophic balance and the temperature is in hydrostatic balance with the vertical pressure gradient.

As in Pedlosky et al., this allows the interior to be completely described in terms of the pressure field. Thus, with:

$$v = p_r, \tag{2.3a}$$

$$T = p_z, \tag{2.3b}$$

the elimination of u and w from Eqs. (2.1b) and (2.1e) and the use of the continuity equation yields as the governing equation for the interior:

$$\left[\frac{1}{r}\frac{\partial}{\partial r}\left(r\frac{\partial}{\partial r}\right) + \frac{1}{\sigma S}\frac{\partial^2}{\partial z^2}\right]\nabla^2 p = 0. \tag{2.4}$$

Note that in the interior, we may write the radial velocity from Eq. (2.1b) as:

$$u = \frac{E}{2}\frac{\partial}{\partial r}\nabla^2 p. \tag{2.5}$$

It is also useful to introduce the stream function for the circulation in the vertical plane as:

$$ru = -\psi_z, \tag{2.6a}$$

$$rw = \psi_r. \tag{2.6b}$$

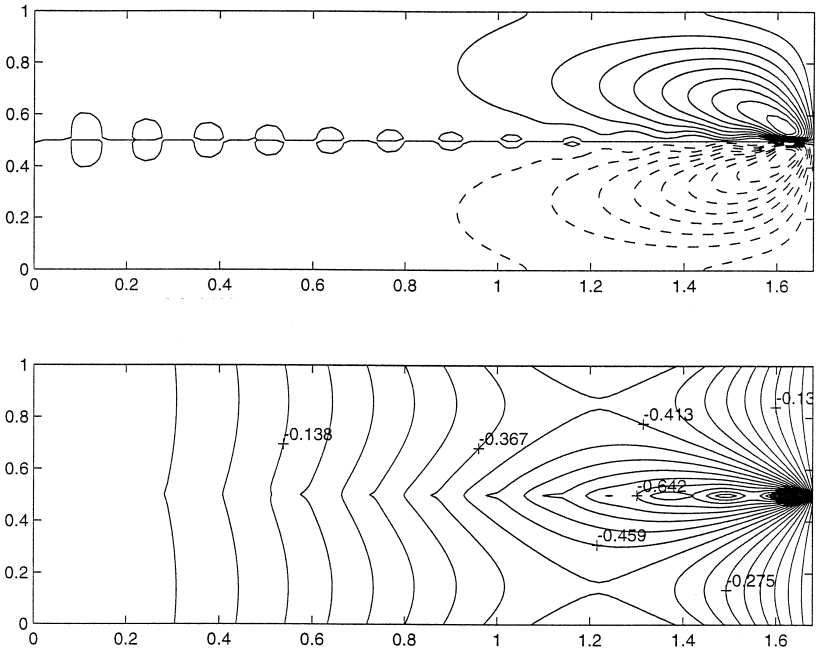

Fig. 2. Top: Azimuthal velocity produced by a point heater located midway along the side boundary. Bottom: Meridional stream function from a point heater. $S = 0.21$; $E = 9.37 \times 10^{-5}$.

The Ekman layers impose a compatibility condition on the interior geostrophic pressure field at the lower and upper boundaries. As in Pedlosky et al., this boundary condition for the interior flow can be written as:

$$\nabla^2 p_z = \mp \frac{\sigma S}{E^{1/2}} \nabla_h^2 p, \quad z = \begin{pmatrix} 1 \\ 0 \end{pmatrix}. \tag{2.7}$$

where

$$\nabla_\eta^2 = \frac{1}{r} \frac{\partial}{0r} r \frac{\partial}{0r}.$$

On the outer rim of the cylinder, a boundary layer called the buoyancy layer exists. The dynamics of this layer is discussed in detail in Barcilon and Pedlosky (1967a) and we do not repeat their analysis here. Suffice it to say that if the *non-dimensional* heating distribution (scaled by Q_j) is given by $H(z)$, the vertical transport in the boundary layer is given by the boundary layer stream function:

$$\hat{\psi} = \frac{E}{\sigma S} \frac{a}{2} H(z) e^{-\eta} (\sin \eta + \cos \eta), \tag{2.8}$$

$\nabla \eta^2 = (a - r)/\delta_b$. Here, a is the non-dimensional radius of the cylinder.

This imposes a condition on the interior stream function at $r = a$. Namely, that on the outer edge of the interior region, the interior stream function must satisfy:

$$\psi_1 = -\frac{E}{\sigma S} \frac{a}{2} H(z), \quad r = a, \tag{2.9}$$

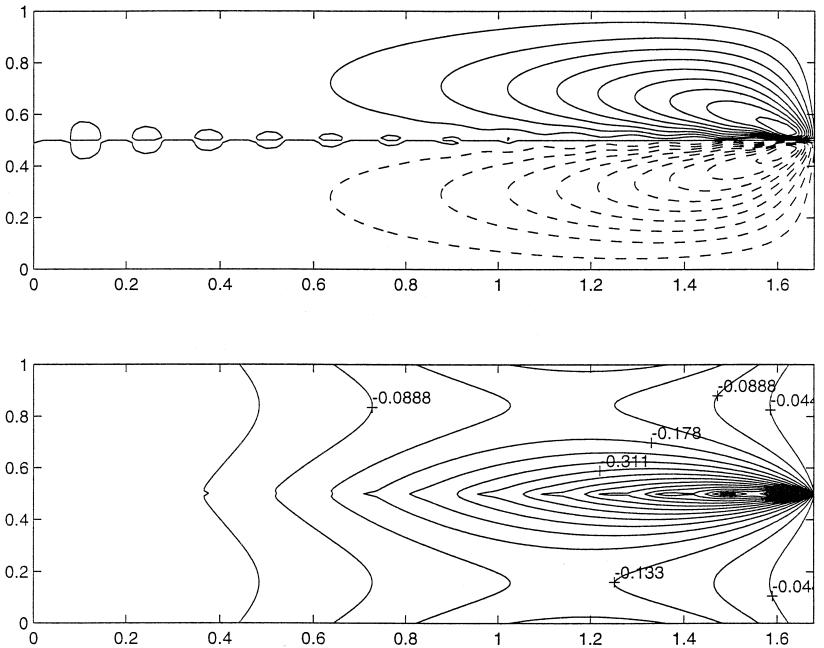

Fig. 3. Top: Azimuthal velocity produced by a point heater located midway along the side boundary. Bottom: Meridional stream function from a point heater. $S = 0.84$; $E = 1.87 \times 10^{-4}$.

corresponding to a weak suction into the boundary layer from the interior given in terms of the imposed heating, i.e.,

$$u = \frac{E}{2\sigma S}\frac{\partial H}{\partial z}. \tag{2.10}$$

This, with Eq. (2.5), yields the final boundary condition on the interior flow, namely that on $r = a$:

$$\frac{\partial}{\partial r}\nabla_{\mathrm{h}}^2 p = \frac{1}{\sigma S}\frac{\partial H}{\partial z}. \tag{2.11}$$

A heat source localized in z will have regions where $\partial H/\partial z$ is both positive and negative, giving rise to regions where the radial velocity is positive and others where it is negative. Where it is positive, we expect the azimuthal velocity to be negative, while in regions where u is negative, we expect v to be positive.

An analysis of the boundary layers on both the bottom and sides of the cylinder also easily shows that the interior pressure field must satisfy directly the no-slip condition on the azimuthal velocity on the side wall so that:

$$\frac{\partial p}{\partial r} = 0 \text{ on } r = a, \tag{2.12}$$

while on the upper and lower boundaries, the interior pressure, through the hydrostatic relation, satisfies:

$$\frac{\partial p}{\partial z} = 0 \text{ on } z = 0,1. \tag{2.13}$$

This problem may be conveniently solved by expanding p in a Fourier–Bessel series:

$$p = \sum_{n=1} P_n(z)\, J_0(k_n r), \tag{2.14}$$

where the set members k_n are chosen to satisfy Eq. (2.12), i.e., they are related to the zeroes of the derivative of the Bessel function of order zero.

This yields an ordinary differential equation for $P_n(z)$, viz.:

$$\frac{\mathrm{d}^4 P_n}{\mathrm{d}z^4} - (\sigma S + 1) k_n^2 \frac{\mathrm{d}^2 P_n}{\mathrm{d}z^2} + k_n^4 \sigma S P_n = -\frac{2}{a J_0(k_n a)} \frac{\partial H}{\partial z}, \tag{2.15}$$

subject to:

$$\frac{\mathrm{d}^3 P_n}{\mathrm{d}z^3} = \pm \frac{\sigma S}{E^{1/2}} k_n^2 Pn, \quad z = \begin{pmatrix} 1 \\ 0 \end{pmatrix}. \tag{2.16}$$

Note that the solutions of the homogeneous part of Eq. (2.15) fall into two classes. Both solutions are exponential in z. The first has a vertical e-folding scale of $1/k_n$ while the

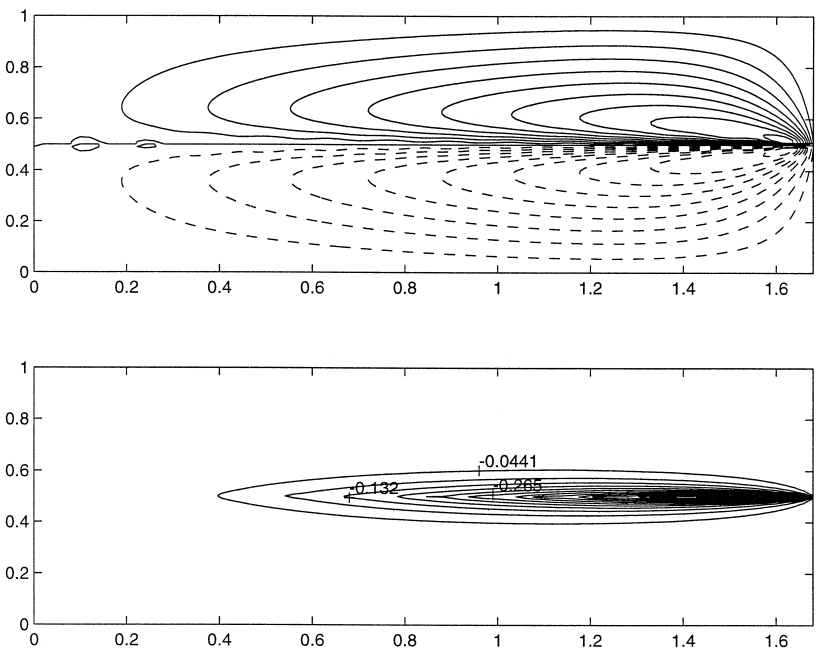

Fig. 4. Top: Azimuthal velocity produced by a point heater located midway along the side boundary. Bottom: Meridional stream function from a point heater. $S = 13.44$; $E = 7.5 \times 10^{-4}$.

second has a vertical e-folding scale $1/k_n(\sigma S)^{1/2}$. The former is a solution of Laplace's equation while the latter is a homogeneous solution of the first operator in Eq. (2.4). Only the latter solution is connected with meridional flow in the vertical plane, i.e. with ψ different from zero.

We consider an idealized heating which is a close representation of the laboratory case in which the heating is concentrated at $z = z_0 = 1/2$. We do this by writing:

$$H = \delta(z - z_0). \tag{2.17}$$

It is straightforward to solve Eq. (2.15) subject to the boundary conditions (2.13) and (2.16) on $z = 0$ and 1. The solution is a sum of exponentials in the regions $z > z_0$ and $z < z_0$ with continuity conditions on the function and its first two derivatives at $z = z_0$ while the jump in the third derivative of P_n is determined by integrating Eq. (2.15) in a small neighborhood about the point $z = z_0$. The technique is standard and we skip the details.

Figs. 2–5 show the principal results of the calculation. They are presented in physical units which correspond to experiments described next. To produce the temperature and velocity scale values, the coefficient of expansion of water at 28°C was used so that profiles in the upper half of the could be compared with experimental data in that region most closely. Unfortunately, non-Boussinesq effects are large in the experiments and

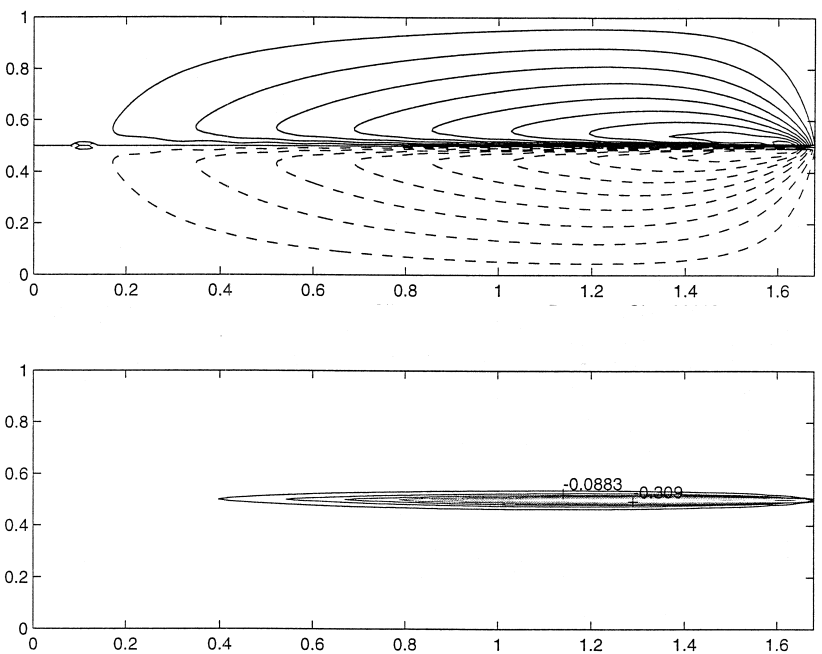

Fig. 5. Top: Azimuthal velocity produced by a point heater located midway along the side boundary. Bottom: Meridional stream function from a point heater. $S = 116.26$; $E = 2.2 \times 10^{-3}$.

close agreement is not expected throughout the entire region. Fig. 2 shows, in the upper panel, the contours of the azimuthal velocity field. For this relatively small value of S (0.21), the radial extent of the meridional circulation is localized near the sidewall of the cylinder and the resulting azimuthal velocity is also so limited. The azimuthal flow consists of prograde flow in the upper part of the cylinder with equal and opposite (retrograde) flow in the lower half of the region. The lower panel shows the stream function. Fig. 3 shows the same fields for a higher value of S (0.84). The stratification has restricted the meridional circulation by squeezing it in the vertical direction and extending it in the radial direction. Figs. 4 and 5 show the same panels for large values of S (13.44 and 116.26). The fields reach far into the interior of the cylinder. The effect of the stratification is also to reduce the size of the meridional secondary circulation (see Eq. (2.10)) and this in turn reduces the size of the azimuthal velocity driven by the secondary circulation. The maximum v falls from a value of about 0.06 in the low S case to a minimum of about 0.01 in the high S case.

3. Laboratory observations of sidewall heated flows

An apparatus was designed to hold a uniformly rotating, thermally stratified cylinder of water subjected to sideways heating. The device (Fig. 6) consisted of a rotating box 48 cm $\times$ 48 cm with 21 cm high Plexiglas sidewalls. The bottom temperature of the box was maintained at a constant value T_b by a 1-cm thick aluminum bottom plate in contact with an isothermal bath. The test fluid, 10.0 cm in depth, was bounded above by a level rectangular lid 44 cm $\times$ 44 cm $\times$ 16 cm fitted down into the box. This lid possessed a flat metal bottom so that the top temperature of the test region could be kept at a constant value by an isothermal bath at a temperature T_t. The lid rested directly on a vertical cylindrical Plexiglas wall 10 cm high with inside diameter 33.5 cm that served as a lateral boundary to the test region. The 5-mm thick wall contained a single loop of nichrome heating wire cemented in a small groove in the inside at exactly mid-depth (5 cm). This wire had an electrical resistance of 3 Ω. It was electrically connected to a precise DC voltage power supply whose voltage could range from 0 to 7.5 V, thus producing power up to 18.75 W. Using a thermal conductivity of Plexiglas of 5×10^{-4} cal s^{-1} °C cm, and for water of 14.3×10^{-4} cal s^{-1} °C cm, we estimate that 74% of the electrical heat was conducted toward the axis, into the test region enclosed by the cylindrical wall, with the rest being conducted outward. The outer region contained water as well; we presume it acts as a relatively motionless stratified fluid whose temperature profile matches the one of the test chamber. To help in this, the Plexiglas sidewalls of the large square box were carefully covered with foam rubber insulation while the entire experiment was spinning and heating up for a period of many hours. The region between the walls of the lid and the inner walls of the container was also stuffed with foam to decrease thermal contact between the experiment and the outside.

The tank and the two baths were mounted on a 1-m diameter rotating turntable with a rotation rate adjustable to 0.001 s^{-1}. Runs were conducted by setting thermostat and voltage values and commencing rotation. Based on both the present and thermocouple measurements in earlier experiments with similar sizes and rotation rates, it is known that the experiments may take 6 h to arrive at a steady state.

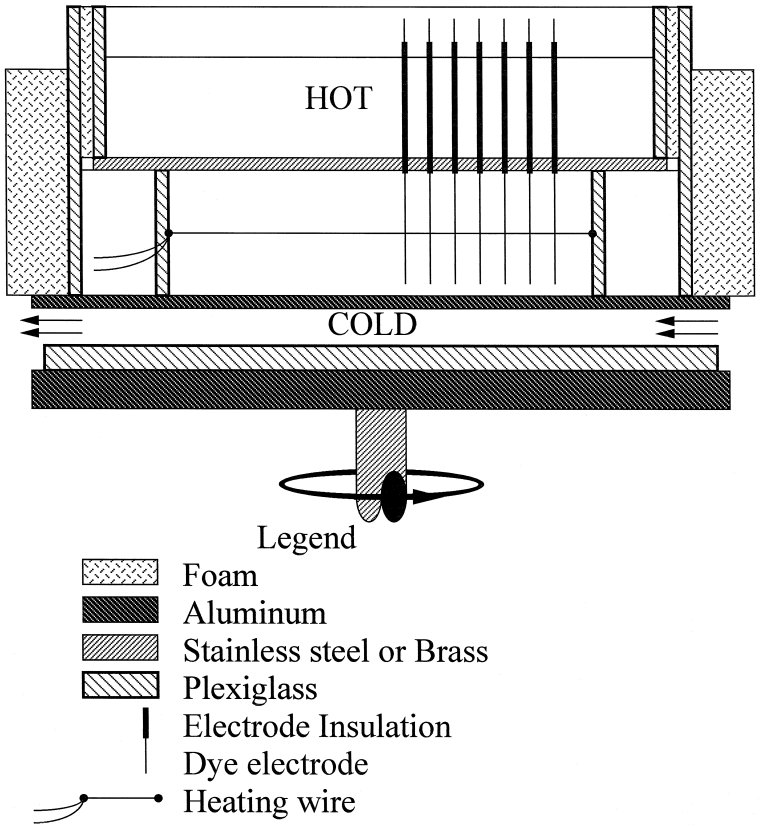

Fig. 6. Apparatus to produce and visualize flows in a rotating stratified fluid with heating from an electric wire located radially at mid-depth at the sidewall. The outer Plexiglas walls are rectangular but the wall with the heating wire is cylindrical.

The flow was visualized using the thymol blue technique. Thymol blue solution, a pH-sensitive indicator, was buffered to the yellow side of its transition pH. The top lid had holes of 0.7 mm diameter through which vertical brass electrodes could be inserted downward into the test fluid. These holes were located at assorted radii from 2 to 14 cm from the center, as shown in Fig. 6. When a voltage (ranging from 1.5 to 4 V depending on stratification strength, flow speed and rotation rate) was applied, the solute around the negative electrode changed to a dark blue with little change of fluid density. The fluid flow was predominantly azimuthal as a consequence of the axial symmetry of the forcing and this velocity was indicated by the motion of the dye away from the wire. This technique is particularly well-suited for measuring slow flows. In the present case, the measured fluid velocities were less than 0.05 cm s^{-1} and this method worked quite well although in a few cases, buoyant effects were noted in the dye after a few minutes.

The principal measured quantity was the azimuthal velocity. During a velocity measurement, the side insulation was removed and the tank was backlit with a white surface illuminated evenly with floodlights. Images of the dye were recorded continu-

ously on video tape as the tank spun in front of the camera. As time progressed, die streaks were swept away from the electrode and a profile could be measured later by freezing video frames and measuring dye displacement. Lengths on the screen were calibrated by adjusting the zoom lens before the experiment so the vertical depth of the test region was full size (10 cm) on the video image. Images were viewed through the flat walls of the box as they rotated into a plane which momentarily became square with the camera view, so there was little image parallax. Thereby, lateral displacements of the dye in the video image corresponded to actual displacement in the fluid. Such a dye profile is shown in Fig. 7, but the image on our monitor was slightly sharper than this reproduction. The dye profile evolved as each electrode rotated into viewing position

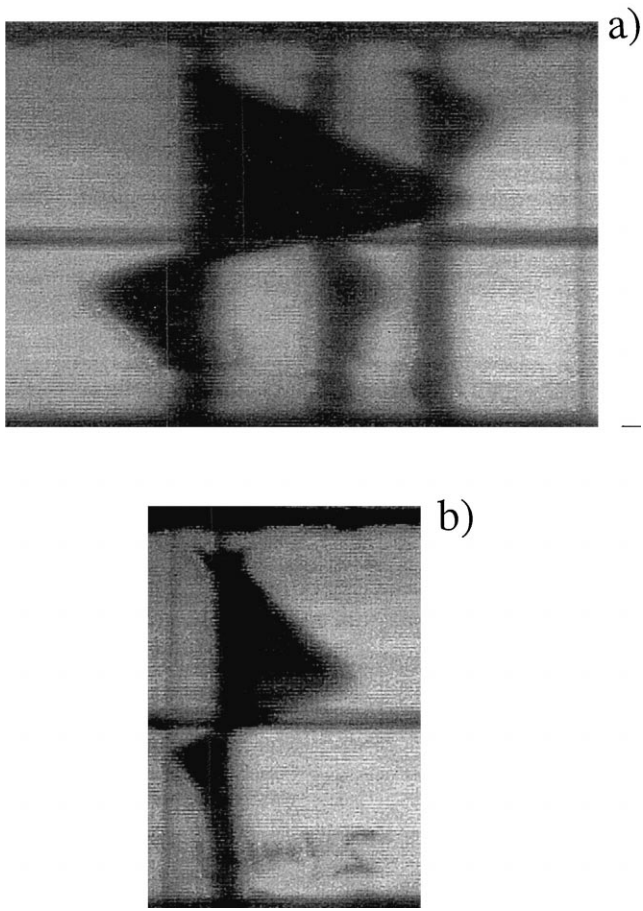

Fig. 7. Photograph of experimental dye profiles. These runs have parameters like the run in Fig. 8f. (a) Profile at a radius of 10 cm. Two profiles at small radii are in the background. (b) Profile at a radius of 12 cm. Note the clear space near the top where the electrode wire is exposed. This is caused by lateral shear in the Ekman layer and descent from the bottom edge of the top Ekman layer. The bottom Ekman layer also has descent and no such clear region is found.

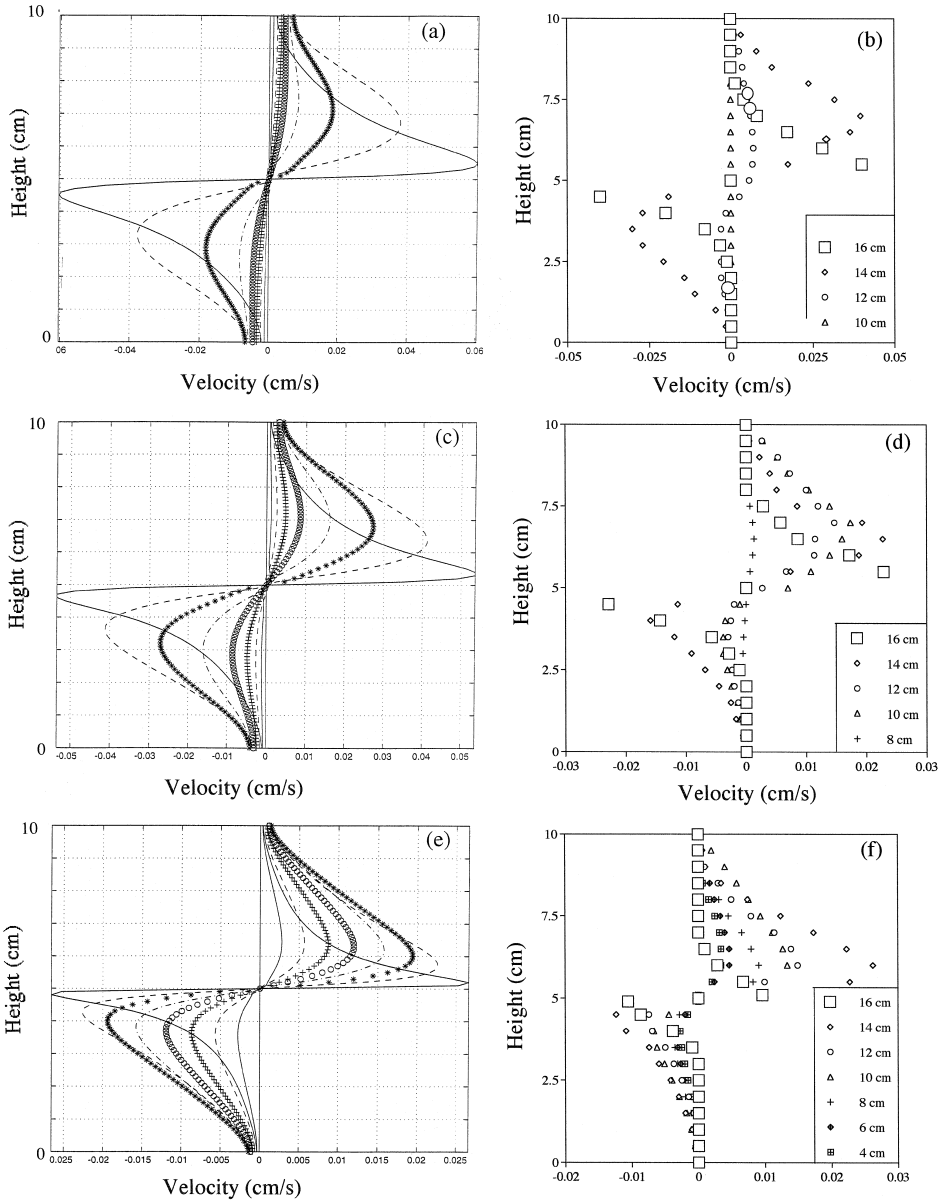

Fig. 8. (a) Profiles of azimuthal velocity at radii of 2 (solid vertical curve), 4 (almost vertical dashed line), 6 (+), 8 (○), 10 (dash–dot), 12 (*), 14 (dashed curve), and 16 (solid curve with greatest velocity) cm from calculations. (b) Profiles at the same radii from direct observations of dye movement in the experiment with small stratification. $S = 0.21$; $E = 9.37 \times 10^{-5}$. Estimated errors for all data are the size of the large squares except for the two squares above and below mid-depth. There, the dye was stretched to invisible levels, so the velocity is much greater than the value reported here. (c), (d) as in (a) and (b) but with $S = 0.84$; $E = 1.87 \times 10^{-4}$. (e), (f) as in (a) and (b) but with $S = 13.44$; $E = 7.5 \times 10^{-4}$. (g), (h) as in (a) and (b) but with $S = 116.2$;, $E = 2.2 \times 10^{-3}$.

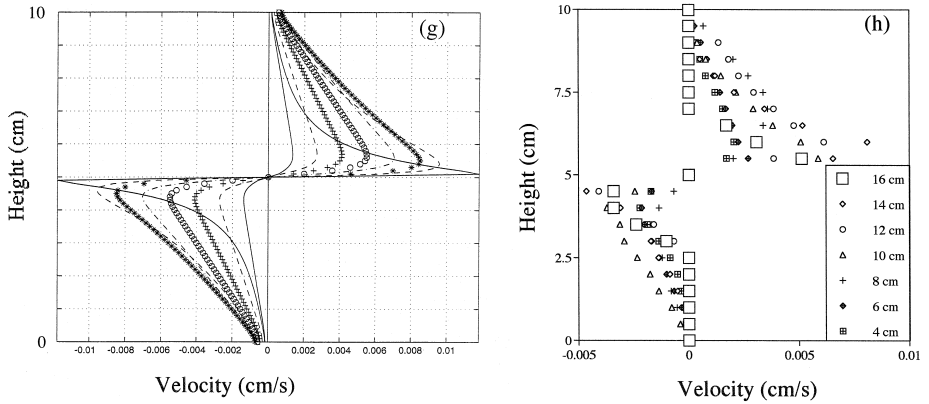

Fig. 8 (continued).

again and again so successive measurements of displacement divided by the time interval between views gave the velocity. The image was traced onto a transparency and digitized from that. Because of the small amount of parallax with the square walls, a view of the meridional velocity could also be obtained by viewing dye near an electrode $1/4$ of a full circle from the position of closest approach to the camera. Such information was only qualitative and no extensive set of quantitative measurements was taken. It was used only to detect the presence of azimuthal instabilities.

Errors in the dyed fluid position measurements are estimated at less than $\pm 5\%$ of the maximum displacement present on the video screen and this is magnitude is illustrated by the size of the square symbols in Fig. 8. Half the error is due to graininess of the screen and lack of information of location of the vertical rod which is somewhat obscured by dye at later times. Some departure from the geostrophic velocity also exists from buoyant effects from tiny electrode heating, tiny bubbles and buoyant effects of the dyed fluid (small double diffusive fingerlike effects were often seen after about 15 min). But there was a third larger uncertainty for the flow near the heater, where displacement was so great that the dye was stretched into an invisible sheet. This uncertainty results in a measurement of a lower bound on the speed as the place where the dye fades to zero. Thus, the lack of agreement of the speed for the 16-cm radius immediately above and below the heater is due to inadequacies in the measurement and not a shortfall of the theory. Agreement between theory and the actual flow may be much better than shown.

Experiments were conducted over a range of values of S from $S = 0.07$ to 116. Values of top and bottom temperatures were kept to an average value of 20°C; their difference is given in Table 1. The parameter S was varied by changing temperature difference and using various rotation rates whose range was dictated by geometric considerations plus, for comparison with theory, the dual needs of small E and Ro. The largest useful value of turntable rotation was limited by centrifugal effects that would negate the planar nature of the top and bottom surfaces. In all cases, E ranged from 0.000066 to 0.002 and therefore was small. Lower rates of rotation might have produced acceptable values of E, but they produced very large Rossby numbers of the flow. Fig. 8

Table 1
Parameters of the experiments

f (s^{-1})	ΔT_v (°C)	Q (W)	E	S	Stability
2.0	30	3.9	10^{-4}	0.21	Y
1.0	30	3.9	2×10^{-4}	0.84	Y
0.25	30	3.9	8×10^{-4}	13.4	Y
0.085	30	3.9	2.2×10^{-3}	116	Y
3.0	30	3.9	6.6×10^{-5}	0.09	N
2.0	20	0.62	10^{-4}	0.14	Y
2.0	20	1.5	10^{-4}	0.14	N
3.0	30	1.5	6.6×10^{-5}	0.09	N
2.0	30	1.5	10^{-4}	0.21	Y
2.0	10	0.62	10^{-4}	0.07	N
2.0	10	0.27	10^{-4}	0.07	N

shows velocity data from stable (axisymmetric) flows with four progressively larger values of S. The left-hand panel in each row shows vertical profiles of azimuthal velocity at even values of radius from the calculations in Section 2; the right-hand panel shows experimental measurements of velocity at assorted depths at the same values of radius. In both theory and measurements, the principal qualitative trend of the flow field extending to smaller radii for larger S was evident. The magnitude of the velocity

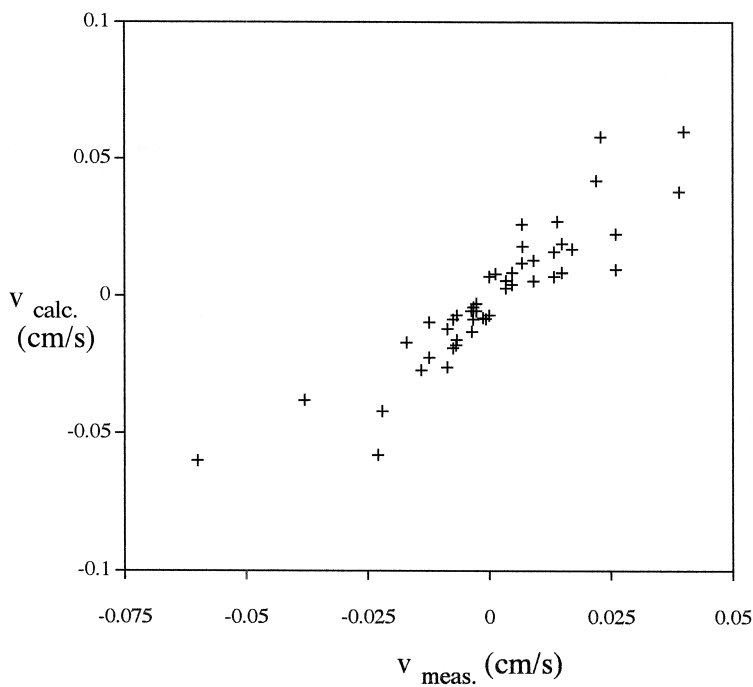

Fig. 9. Calculated and measured velocity maxima from the profiles shown in Fig. 8.

profiles and the vertical extent of velocity matched particularly well near the heat source except for the profile right next to the heater, where the velocity peak was lost due to the smearing of dye as discussed above. In general, there is good correspondence between calculations and measurements at larger radii, but at smaller radii, the correspondence is poorer and in some cases, measurements tend to be smaller than calculations by factors more than 2.

Quantitative comparison between calculation and theory for all the data in the preceding figure is shown by Fig. 9, in which the velocity of the maxima from theory is plotted against the maxima from the experimental data. As in the earlier studies by Pedlosky et al., there was scatter about the perfect fit. In this case, the correlation coefficient is 0.91. The poorest correlation was for the data with greatest measurement problems mentioned above.

The remainder of the runs in Table 1 were conducted to document parameters for a departure from axisymmetry that was found first in the run reported in the fifth row. Little is known of this instability except that dye patterns clearly departed from the orderly profiles shown in Fig. 8. In addition, radial displacements of the dye was clearly visible in the container. Except for noting the existence of a possible instability, and documenting that it happens for more rapid rotation and larger values of heating, investigation awaits further efforts.

4. Discussion

Let us briefly review the boundary layer sizes for these problems using Cartesian coordinates. The governing equation is found by using the Cartesian equivalents of Eqs. (2.1a), (2.1b), (2.1c), (2.1d) and (2.1e) using L for the depth of the region and R for the width. It is:

$$\nabla^2\left[\left(\nabla^2\right)^3 v + \frac{4\sigma S\varepsilon^2}{E^2} v_{xx} + \frac{4}{E^2} v_{zz}\right] = 0, \tag{4.1}$$

with $\nabla^2 = \varepsilon^2(\partial^2/\partial x^2) + (\partial^2/\partial z^2)$ and $\varepsilon = L/R$. The three possible boundary layers on the top and bottom surfaces for small E are found by balancing the highest order z-derivative in the first and third, first and second, and second and third terms, respectively, with the further assumption that the lateral derivative is order one. Their sizes are:

$$b_{t1} = \sqrt{\frac{E}{2}}\,, \tag{4.2a}$$

$$b_{t2} = \sqrt[6]{\frac{E^2}{4\sigma S\varepsilon^2}}\,, \tag{4.2b}$$

$$b_{t3} = \sqrt{\frac{1}{\sigma S\varepsilon^2}}\,. \tag{4.2c}$$

The parameter group $\sigma S\varepsilon^2$ appears together, and it is instructive to examine the size of the boundary layers for progressively larger $\sigma S\varepsilon^2$. As it is progressively increased from zero (for which only Ekman layers are found), the second and third boundary layer sizes (Eqs. (4.2b) and (4.2c)) are greater than one, so they occupy the entire fluid region. The second boundary layer becomes smaller than the Ekman layer for $\sigma S\varepsilon^2 > 2/E$, and it is easy to show that in that range, all three terms in Eq. (4.1) involving the highest order z-derivative are of equal magnitude so the third boundary layer will also be dynamically active. Thus, one can consider the Ekman layer to split onto the second and third boundary layers above that limit. This split is similar to the splitting of the sidewall boundary layer into two boundary layers noted by Barcilon and Pedlosky (1967b) in (Fig. 1). The experiments and analysis of Pedlosky et al. (1997), in which differential heating was applied to the top of a cylinder of thermally stratified rotating water, illustrate the roles of such boundary layers over a wide range of S. Their well-known dimensional sizes are:

$$b_{\mathrm{td}1} = \sqrt{\frac{\mu}{\rho f}}\,, \tag{4.3a}$$

$$b_{\mathrm{td}2} = \left(\frac{\mu R}{\rho\sqrt{\sigma}N}\right)^{1/3}, \tag{4.3b}$$

$$b_{\mathrm{td}3} = \frac{Rf}{\sqrt{\sigma}N}, \tag{4.3c}$$

respectively. None depends on the depth of the cylinder but two depend on the lateral size R. We have conducted calculations not reported here which produce these boundary layers in a Cartesian system driven by sinusoidal forcing on the top surface in a semi-infinite layer. They reveal that the wavelength of the thermal forcing can be substituted for R.

The sidewall boundary layers are found by balancing the highest order x-derivatives in the first and third, first and second, and second and third terms, respectively, with the further assumption that the vertical derivative is order one. This latter assumption is not correct for the heat source of our present experiment, and the consequences of localized sidewall heating will be discussed later. The boundary layers are of size:

$$b_{\mathrm{s}1} = \varepsilon\sqrt[3]{\frac{E}{2}}\,, \tag{4.4a}$$

$$b_{\mathrm{s}2} = \varepsilon\sqrt{\frac{E}{2\sqrt{\sigma S}}}\,, \tag{4.4b}$$

$$b_{\mathrm{s}3} = \varepsilon\sqrt{\sigma S} \tag{4.4c}$$

As σS increases from zero, the first boundary layer (Eq. (4.4a)), since its balance involves the first and third terms of Eq. (4.1), and the second term are smaller. At $\sigma S = (E/2)^{2/3}$, the second term becomes as large as the other two and all three boundary layers have the same size. For $\sigma S > (E/2)^{2/3}$, the two layers of sizes

(Eqs. (4.4b) and (4.4c)) are dynamically active together, so that one could picture that the first layer has split into the second two. For $\varepsilon\sqrt{\sigma S} > 1$, Eq. (4.4c) becomes greater than one and the dynamical balance that involves that boundary layer occupies the entire interior of the fluid. The dimensional sizes of the above three boundary layers and their ranges of validity are:

$$b_{\mathrm{sd}1} = \sqrt[3]{\frac{\mu L}{\rho f}} \quad \text{for } \sigma S < \left(\frac{E}{2}\right)^{2/3}, \text{ otherwise,} \tag{4.5a}$$

$$b_{\mathrm{sd}2} = \sqrt{\frac{\mu}{\rho\sqrt{\sigma} f}}, \tag{4.5b}$$

$$b_{\mathrm{sd}3} = \frac{\sqrt{\sigma} NL}{f}. \tag{4.5c}$$

None depends on lateral length R but two depend on the depth of the container L.

Calculations were performed using Eq. (4.1) to clarify the role of localized heating. A boundary condition for one variable (u, v, T, or w), which was sinusoidal in the z-direction, was imposed at $x = 0$ and all variables were set to zero at $x = 1$. This formulation is equivalent to the physical situation of a vertical slot of rotating stratified fluid which is infinite in the vertical and flow directions with a sinusoidal forcing in the vertical direction imposed along one wall. All variables have zero deviations from linear uniform stratification along the other wall. The results showed that the wavelength of the forcing λ can be used instead of the depth of the container for the vertical length scale L. The gap width of the slot was found to not effect the boundary layer sizes, a result consistent with R not appearing in Eqs. (4.5a), (4.5b) and (4.5c). Point heaters on a sidewall stacked over each other with spacing λ would be represented by a Fourier series with each harmonic of equal amplitude. Thus, the first and third boundary layer thicknesses in Eqs. (4.5a), (4.5b) and (4.5c) varied with each Fourier component but the second did not.

These features are contained in the analysis of Section 2, but they may not be readily apparent since the method of solutions does not separate out the role of the harmonic composition of the boundary layers explicitly. Instead, the method can be considered to yield the flows produced by a Green's function located along the wall. Thus, flows from more complicated heater distributions could be found by integrating the present solutions over a distribution of point heaters using known concepts.

5. Concluding remarks

The above experiments and theoretical considerations show how the combined effects of stratification and fluid rotation act on steady linearized flows driven by sidewall heating. A variety of boundary layers are possible. The effects of some of these boundary layers have been documented in laboratory observations in combination with analytical solutions for flow in a cylinder. Generally speaking, such boundary layers allow vertical thermally driven flows near both vertical and lateral boundaries, which can then lead to interior temperature distributions that will produce thermal wind

motions. Laplace's equation relates azimuthal flow to thermal perturbations through thermal wind. If forcing has sufficiently long length scale, both temperature and azimuthal velocity can penetrate into the interior of rotating strongly stratified fluid. But in some ranges, vertical and radial (or, in Cartesian coordinates, lateral) velocity is confined to a boundary layer region whose vertical extent is $b_{\mathrm{td3}} = (Rf/\sqrt{\sigma}N)$ where R is the length scale of radial (lateral) forcing, or equivalently whose lateral extent is $b_{\mathrm{sd3}} = (\sqrt{\sigma}NL/f)$ where L is the length scale of vertical forcing.

Acknowledgements

Support for the calculations was provided by NSF Grant no. OCE 9301845, and for the laboratory experiment by the Office of Naval Research with grant no. N00014-97-1-0195. The construction of the apparatus by John Salzig is very gratefully acknowledged. Contribution no. 9822 of the Woods Hole Oceanographic Institution.

References

Aagard, K., 1981. On the deep circulation in the Arctic ocean. Deep-Sea Res. 28A, 251–268.

Barcilon, V., Pedlosky, J., 1967a. Linear theory of rotating stratified fluid motions. J. Fluid Mech. 29, 1–16.

Barcilon, V., Pedlosky, J., 1967b. A unified linear theory of homogeneous and stratified rotating fluids. J. Fluid Mech. 29, 609–621.

Barcilon, V., Pedlosky, J., 1967c. On the steady motions produced by a stable stratification in a rapidly rotating fluid. J. Fluid Mech. 29, 673–690.

Bennett, J.R., 1975. Another explanation of the cyclonic circulation of large lakes. Limnol. Oceanogr. 20, 108–110.

Bulgakov, S.N. 1987. Investigation of the haline factors role in the Black Sea circulation and water structure formation. PhD Thesis, Marine Hydrophysical Institute, Sevastopol, USSR, 155 pp.

Bulgakov, S.N., Korotaev, G., 1987. Mar. Hydrophys. J., 14–21.

Bulgakov, S.N., Korotaev, G.K., Whitehead, J.A., 1996a. The role of buoyancy fluxes in the formation of a large-scale circulation and stratification of sea water: 1. The theory. Izv. Atmos. Ocean Phys. 32, 548–556, in Russian.

Bulgakov, S.N., Korotaev, G.K., Whitehead, J.A., 1996b. The role of buoyancy fluxes in the formation of a large-scale circulation and stratification of sea water: 2. Laboratory experiments. Izv. Atmos. Ocean Phys. 32, 557–564, in Russian.

Chao, S.-L., 1988. River-forced estuarine plumes. J. Phys. Oceanogr. 18, 72–88.

Chao, S.L., Boicourt, W., 1986. Onset of estuarine plume. J. Phys. Oceanogr. 16, 2137–2149.

Chapman, D.C., Lentz, S.J., 1994. Trapping of coastal density front by the bottom boundary layer. J. Phys. Oceanogr. 24, 1464–1479.

Chapman, D.C., Lentz, S.J., 1996. Adjustment of stratified flow over a sloping bottom. J. Phys. Oceanogr. 27 (2), 340–356.

Csanady, G.T., 1976. Mean circulation in shallow seas. J. Geophys. Res. 81, 5389–5399.

Csanady, G.T., 1977. On the cyclonic mean circulation of large lakes. Proc. Natl. Acad. Sci. U.S.A. 74, 2204–2208.

Emery, K.O., Csanady, G.T., 1973. Surface circulation of lakes and nearly land-locked seas. Proc. Natl. Acad. Sci. U.S.A. 70, 93–97.

Garvine, R.W., 1974. Physical features of the Connecticut river outflow during high discharge. J. Geophys. Res. 79, 831–846.

Garvine, R.W., 1987. Estuary plumes and fronts in shelf waters: a layer model. J. Phys. Oceanogr. 17, 1877–1896.

Garvine, R.W., 1996. Buoyant discharge on the inner continental shelf: a frontal model. J. Mar. Res. 54, 1–33.
Gill, A.E., 1976. Adjustment under gravity in a rotating channel. J. Fluid Mech. 77, 603–621.
Griffiths, R.W., 1986. Gravity currents in rotating systems. Annu. Rev. Fluid Mech. 18, 59–86.
Griffiths, R.W., Hopfinger, E.J., 1983. Gravity currents moving along a lateral boundary in a rotating fluid. J. Fluid Mech. 134, 357–393.
Johnson, G.C., 1998. Deep water properties, velocities, and dynamics over ocean trenches. J. Mar. Res. 56, 329–347.
Johnson, G.C., Sanford, T.B., Baringer, M.O., 1994a. Stress on the mediterranean outflow plume: I. Velocity and water property measurements. J. Phys. Oceanogr. 24 (10), 2072–2083.
Johnson, G.C., Lueck, R.G., Sanford, T.B., 1994b. Stress on the mediterranean outflow plume: II. Turbulent dissipation and shear measurements. J. Phys. Oceanogr. 24 (10), 2084–2092.
Jungclaus, J.H., Backhaus, J.O., 1994. Application of a transient reduced gravity plume model to the Denmark strait overflow. J. Geophys. Res. 99 (C6), 12375–12396.
Kourafalou, V.K., Oey, L.-Y., Wang, J.D., Lee, T.N., 1996. The fate of river discharge on the continental shelf: 1. Modeling the river plume and the inner shelf coastal current. J. Geophys. Res. 101, 3415–3434.
Krysell, M., Wallace, D.W.R., 1988. Arctic ocean ventilation studied with a suite of anthropogenic halocarbon tracers. Science 242, 746–749.
Latif, A., Ozsay, E., Oguz, T., Unluata, U., 1991. Observations of the mediterranean inflow into the Black sea. Deep-Sea Res. 38 (2), 5711–5723, Suppl.
Masse, A.K., Murthy, C.R., 1992. Analysis of the Niagara river plume dynamics. J. Geophys. Res. 97, 2403–2420.
Munchow, A., Garvine, R.W., 1993. Dynamical properties of a buoyancy-driven coastal current. J. Geophys. Res. 98, 20063–20077.
O'Donnell, J., 1990. The formation and fate of a river plume: a numerical model. J. Phys. Oceanogr. 20, 551–569.
Pedlosky, J., 1979. Geophysical Fluid Dynamics. Springer-Verlag, New York, 624 pp.
Pedlosky, J., Whitehead, J.A., Veitch, G., 1997. Thermally driven motions in a rotating stratified fluid: theory and experiment. J. Fluid Mech. 339, 391–411.
Price, J.F., Baringer, M.O., Lueck, R.G., Johnson, G.C., Ambar, I., Parrilla, G., Cantos, A., Kennelly, M.A., Sanford, T.B., 1993. Mediterranean outflow mixing and dynamics. Science 259, 1277–1282.
Smith, P.C., 1975. A stream tube model for bottom boundary currents in the ocean. Deep-Sea Res. 22, 853–873.
Spall, M.A., Price, J.F., 1998. Mesoscale variability in Denmark Strait: the PV outflow hypothesis. J. Phys. Oceanogr. 28, 1598–1623.
Stalcup, M.C., Matcalf, W.G., Johnson, R.G., 1975. Deep Caribbean inflow through the Anegada–Jungfern passage. J. Mar. Res. 33, 15–35, Suppl.
Stern, M.E., 1980. Geostrophic fronts, bores, breaking and blocking waves. J. Fluid Mech. 99, 687–703.
Stern, M.E., Whitehead, J.A., Hua, B.-L., 1982. The intrusion of a density current along the coast of a rotating fluid. J. Fluid Mech. 123, 237–265.
Sturges, W., 1975. Mixing of renewal water flowing into the Caribbean sea. J. Mar. Res. 33, 117–130, Suppl.
Takano, K., 1955. A complimentary note on the diffusion of the seaward river flow off the mouth. J. Oceanogr. Soc. Jpn. 11, 1–3.
Veronis, G., 1967. Analogous behavior of rotating and stratified fluids. Tellus 19, 620–634.
Wang, D.P., 1987. The strait surface outflow. J. Geophys. Res. 92, 10807–10825.
Whitehead, J.A., 1989. Giant ocean cataracts. Sci. Am. 260, 50–57.
Whitehead, J.A., Chapman, D.C., 1986. Laboratory observations of a gravity current on a sloping bottom: the generation of shelf waves. J. Fluid Mech. 172, 373–399.
Whitehead, J.A. Jr., Miller, A.R., 1979. Laboratory simulation of the gyre in the Alboran sea. J. Geophys. Res. 84 (C7), 3733–3742.
Whitehead, J.A., Korotaev, G.K., Bulgakov, S.N., 1998. Convective circulation in mesoscale abyssal basins. Geophys. Astrophys. Fluid Dyn. 89 (34), 169–203.
Wunsch, C., 1973. On mean drift in large lakes. Limnol. Oceanogr. 18, 793–795.
Yankovsky, A.E., Chapman, D.C., 1997. A simple theory for the fate of buoyant coastal discharges. J. Phys. Oceanogr. 27, 1386–1401.